Phonon contribution to electrical resistance of acceptor-doped single-wall carbon nanotubes assembled into transparent films

V. I. Tsebro,[1,*] A. A. Tonkikh,[2,3] D. V. Rybkovskiy,[2,3] E. A. Obraztsova,[4,†] E. I. Kauppinen,[5] and E. D. Obraztsova[2]

[1]*P. N. Lebedev Physical Institute, Russian Academy of Sciences, 53 Leninsky Prospect, 119991 Moscow, Russia*
[2]*A. M. Prokhorov General Physics Institute, Russian Academy of Sciences, 38 Vavilov Street, 119991 Moscow, Russia*
[3]*Faculty of Physics, Southern Federal University, 5 Zorge Street, 344090 Rostov-on-Don, Russia*
[4]*Shemyakin and Ovchinnikov Institute of Bioorganic Chemistry, Russian Academy of Sciences,*
16/10 Miklukho-Maklaya Street, 117871 Moscow, Russia
[5]*Department of Applied Physics, Aalto University, School of Science, Post Office Box 15100, FI-00076 Espoo, Finland*

The electrical resistance of pristine and acceptor-doped single-wall carbon nanotubes assembled into transparent films was measured in the temperature range of 5 to 300 K. The doping was accomplished by filling the nanotubes with iodine or CuCl from the gas phase. After doping the films resistance appeared to drop down by one order of magnitude, to change the nonmonotonic temperature behavior, and to reduce the crossover temperature. The experimental data have been perfectly fitted in frames of the known heterogeneous model with two contributions: from the nanotube bundles (with quasi-one-dimensional conductivity) and from the interbundle electron tunneling. The doping was observed to decrease the magnitudes of both contributions. In this paper we have revealed the main reason of changes in the nanotube part. It is considered to be connected with the involvement of low-energy phonons, which start to participate in the intravalley scattering due to the shift of the Fermi level after doping. The values of the Fermi level shift into the valence band are estimated to be equal to -0.6 eV in the case of iodine doping and -0.9 eV in the case of CuCl doping. These values are in qualitative agreement with the optical absorption data.

I. INTRODUCTION

Transparent conducting netlike single-wall carbon nanotube (SWCNT) films are promising candidates for the production of transparent electrodes for photovoltaic devices, displays, and other optoelectronic applications [1–9]. The conducting framework of such electrodes consists of a SWCNT network with metallic (M) and semiconducting (S) nanotubes [10,11] in the approximate ratio of 1:2 [12]. For practical application, industry specification for transparent conducting films requires transparencies higher than 90% and sheet resistance R_{sq} lower than 90 ohm/sq (see, e.g., [13]). The highly transparent (80–90%) SWCNT films formed from pristine nanotubes with noticed M/S ratio have the values of R_{sq} ranging from unacceptable values (10^3–10^4 ohm/sq) [2,8] to those (89–310 ohm/sq)[4,14–16] which are in close proximity to required ones. The sheet resistance of pristine SWCNT films depends on the purity of the samples, the length and diameter of the nanotubes, and the size of the SWCNT bundles [13,15]. The best value of $R_{sq} = 89$ ohm/sq has been obtained for 90%-transparent SWCNT films fabricated using aerosol technology, which leads to an almost complete elimination of SWCNT bundling (known for such technique as arc discharge [17]) and a substantial increase in SWCNT lengths via the suppression of bundling-induced growth termination [16].

The sheet resistance of SWCNT films can be significantly decreased by acid(HNO_3) treatment that results in a high level of p-type doping [9,14,18,19]. The other examples of strong acceptors for p-type doping are iodine and cuprous chloride (CuCl) [20–24]. The iodine-doped SWCNT films may have the value of R_{sq} as low as 70 ohm/sq [22]. The conducting properties of CuCl-doped samples have been less investigated, but preliminary results show $R_{sq} < 100$ ohm/sq [23,24]. As a result of gas-phase doping, which we used earlier in Ref. [25], the one-dimensional (1D) iodine and CuCl structures are formed inside nanotubes or between nanotubes in the bundles [26–28]. The form of these structures depends on the nanotube diameter, and the degree of charge transfer from nanotubes to the dopants increases in value with the tube diameter [22]. For nanotubes with an average diameter equal to or higher than 2 nm, the temperature dependence of electrical resistance $R(T)$ of iodine-doped SWCNT films in the range of 100 to 300 K has a positive coefficient ($dR/dT > 0$) corresponding to metallic conductivity [22].

The significant decrease of electrical resistance of SWCNT films after doping is an inevitable result of the Fermi level shift into the region of Van Hove peaks in the electron density of states (DOS) in the valence band, which leads to the metallization of the semiconducting portion of nanotubes and a sharp increase of the film conductivity.

This work represents an attempt to interpret the nanotube contribution in the total resistance of transparent SWCNT films, and to get a quantitative result of Fermi level shifting by analyzing the temperature dependencies ($5 < T < 300$ K) of pristine, iodine-doped, and CuCl-doped highly transparent SWCNT films with an average nanotube diameter about 2 nm. For this purpose the known heterogeneous model [29,30] is used. The conducting channels in this model are the long

---
[*]P. L. Kapitza Institute for Physical Problems, Russian Academy of Sciences, 2 Kosygina Street, 119334 Moscow, Russia; v.tsebro@mail.ru

[†]A. M. Prokhorov General Physics Institute, Russian Academy of Sciences, 38 Vavilov Street, 119991 Moscow, Russia.

bundles of nanotubes with a quasi-1D type of conductivity and some paths inside them connected among themselves by tunneling. In this approach, (a) the nanotube contribution in the total resistance is succeeded to be described in terms of the phonon constraint in the process of charge carriers backscattering; (b) the role of low-energy phonons in this process is revealed; and (c) the values of the Fermi level shift into the valence band are determined in doped SWCNT films.

In frames of the heterogeneous model it was also possible to estimate the effect of doping on the intertube tunneling contribution to the electrical resistance of the nanotube films. This question is very important since from the general consideration it is clear that the tunneling contribution to the overall electrical resistance is dominant. This is also evidenced from the results of direct measurements of the contact resistance between the bundles of nanotubes [31]. The results of our work show that doping of nanotube films significantly reduces both the tunneling and the nanotube contributions to the resistance.

II. TRANSPARENT SWCNT FILMS AND EXPERIMENTAL DETAILS

The highly transparent netlike films were prepared from SWCNT of average diameter about 2 nm synthesized by an aerosol technique [32]. During synthesis process the bundles of SWCNT are collected at the reactor bottom onto the nitrocellulose filter with a very weak adhesion. It permits the transparent SWCNT films to be reprinted onto various substrates [9] as, for example, quartz substrates used in our case. Next, the reprinted films were subjected to special treatment in vapors of iodine or the CuCl to fill the nanotube internal channels with vapor molecules and obtain the doped SWCNT films. This doping method is described in detail in Refs. [22,33] for the iodine-doped films, and in Ref. [34] for the CuCl-doped ones. The statistical estimation made by the HR-TEM showed up to 40% filling level of SWCNTs. As was early noted in Ref. [22], the doping of SWCNT films from the gaseous phase does not change in general the morphology of nanotubes and nanotube net that allows us to compare the optical and conducting properties of the films before and after doping with different dopants.

In the present work two sets of the SWCNT netlike films with transparencies of about 90 and 70% were prepared and investigated (the values of transparency were measured at the wavelength of 514 nm). The transparency values were tuned by thickness of the films which did not exceed 100 nm. Scanning electron microscopy (SEM) images of transparent netlike SWCNT films from both sets are shown in Fig. 1.

The optical ultraviolet-visible-near infrared (UV-vis-NIR) measurements within spectral range 500–3000 nm were performed using a spectrophotometer Lambda-950 (Perkin-Elmer). The spectra obtained for pristine films, the iodine-doped films, and the CuCl-doped films with the optical transparency of about 70% are shown in Fig. 2. It is seen that while doping the Burstein-Moss effect [35,36] occurs that is expressed in suppression of the optical transitions E_{11S}, E_{22S}, and E_{11M} by reason of the Fermi level shift deeply into the valence band. The average diameter of nanotubes, $d \approx 2$ nm, as it is generally agreed, was determined according to well-known $E_{\nu\nu}$ dependencies upon the nanotube diameter [37–39].
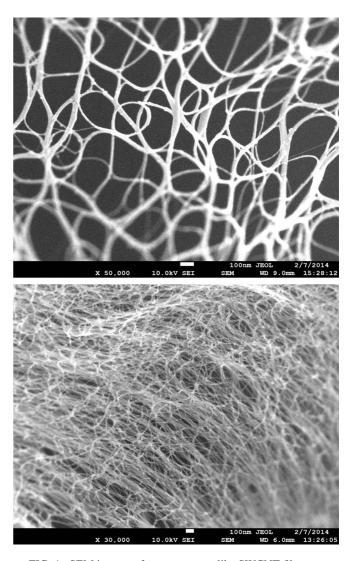

FIG. 1. SEM images of transparent netlike SWCNT films grown by the aerosol technique and having the optical transparency of about 90% (upper image) and 70% (lower image).
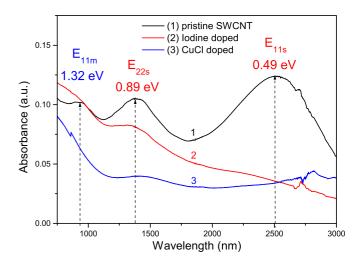

FIG. 2. Optical absorption spectra for (1) pristine films, (2) the iodine-doped films, and (3) films doped with CuCl. The optical transparency is ≈70%.

TABLE I. R_{sq} values (in ohm units) at room temperature depending upon the optical transparency for pristine films and films doped by iodine or CuCl.

Transparency	Pristine	Iodine doped	CuCl doped
$\approx 70\%$	147 ± 21	31 ± 4	28 ± 4
$\approx 90\%$	863 ± 122	151 ± 21	98 ± 14

The measurements of electrical resistance R and its temperature dependencies $R(T)$ for SWCNT films placed onto quartz substrates were carried out by standard dc four-probe method, using a sensitive nanovoltmeter and switchable current source. The substrate with a film 4×10 mm in size was fixed in a special massive holder. The current and voltage contacts to the film were made from the annealed copper wire, 30 μm in diameter, and attached to the film with a self-solidifying paste. The holder with a sample was placed in a blown-through helium cryostat for intermediate temperatures ($5 < T < 300$ K). The temperature dependencies $R(T)$ were measured at slow step-by-step annealing of the holder during which the measuring current changed the direction to exclude the contacts and thermal emf signals. As a rule the total curve $R(T)$ contained about 8000 points. The values of measuring current ranged from 0.1 to 0.5 μA depending on the film resistance. The R_{sq} values were calculated from the ratio $R_{sq} = R\,\omega/l$, where R is the resistance measured, ω is the width of the film, and l is the distance between the voltage contacts.

III. EXPERIMENTAL DATA

The values of R_{sq}, measured at room temperature for pristine, iodine-doped, and CuCl-doped SWCNT films are given in Table I. As seen from these data the biggest R_{sq} drop is in the case of CuCl doping. Under transparency about 90% the value of R_{sq} for these films is comparable with that of a widely used material for transparent conductive films—indium tin oxide [9]. It should be noted that the conducting properties of investigated SWCNT films had no aging effect. The special test showed no R_{sq} difference after air storing the films during one year.

The normalized resistance $R(T)/R(300$ K) of SWCNT films with the different values of optical transparency ≈ 90 and $\approx 70\%$ for pristine film and films doped by iodine or CuCl is shown in Fig. 3. As seen from the data presented the curves $R(T)/R(300$ K) for every set (pristine, iodine doped, and CuCl doped) are very much similar regardless of the film transparency. It points to a single nature of electronic transport in investigated SWCNT films. The temperature dependencies of the electrical resistance are nonmonotonic with a well-defined minimum. The depth of this minimum is increased while its position is shifted to lower temperatures for a stronger acceptor.

The mathematical treatment of the data obtained revealed that in the temperature range of 5 to 300 K the electrical resistance of both pristine and doped SWCNT films is well described by the known heterogeneous model suggested in Refs. [29,30]. In accordance with this model the electri-
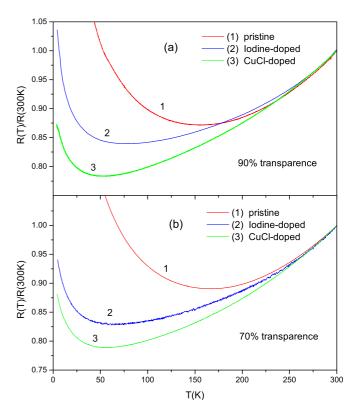

FIG. 3. The normalized resistance of SWCNT films with the different values of optical transparency: $\approx 90\%$ (a) and $\approx 70\%$ (b) for pristine film (1), the iodine-doped film (2), and for the CuCl-doped film (3). The resistance minimum shift toward lower temperatures is seen.

cal resistance consists of two contributions. The first one is determined by the fluctuation-assisted tunneling (FAT), considered in Ref. [40] for the systems with well-conducting mesoscopic regions connected by electronic tunneling through nonconducting material. As was shown in Ref. [40], the conductivity of such a system is conditioned by the fluctuations in the voltage across the tunneling junctions between conducting regions (in our case, conducting bundles of SWCNT).

The second contribution is associated with the proper conductivity of SWCNT bundles in the films. This conductivity has quasi-one-dimensional character, and its behavior is described in terms of the model in which backscattering of the charge carriers by phonons at low temperatures is suppressed [41]. Because the charged dopants in doped SWCNT bundles (or the charged defects and impurities in undoped ones) are spatially separated from the quasi-1D conducting paths, backscattering of the charge carriers, when their wave vector changes within the value of $2k_F$ (k_F is the electronic wave vector), is suppressed, and even relatively weak coupling between conducting paths is sufficient to avoid one-dimensional localization (see Ref. [41] for the case of conducting polymers). As a result, at low temperatures the electrical resistance of SWCNT films is exponentially small because of a very small number of thermally excited $2k_F$ phonons. This number is proportional to $\exp(-\hbar\omega_0/k_B T)$, where ω_0 is the frequency of backscattering phonons.

The heterogeneous model [29,30] is assumed to consider several conducting paths with different conductivity types. The total resistivity of the considered system can be written as [42]

$$\rho(T) = \sum_i \frac{L_i S}{L S_i} \rho_i(T), \qquad (1)$$

where L and S are the total effective length and cross-sectional area of the specimen, L_i is the length of the path which passes through the material of one type with intrinsic resistivity $\rho_i(T)$, and S_i is the effective cross-sectional area of this path. In our case of SWCNT films the sum in Eq. (1) consists of at least two terms. The first one is related to the conducting SWCNT bundles. In the simplest case of one conducting channel with participation of single-type backscattering $2k_F$ phonons with frequency ω_0 it is defined by

$$\rho_1(T) = \rho_m \exp\left(-\frac{\hbar\omega_0}{k_B T}\right) = \rho_m \exp\left(-\frac{T_m}{T}\right),$$

where ρ_m is independent of the temperature constant. If the number of conducting channels in SWCNT bundles is more than one, and each of these channels has again the peculiar frequency of $2k_F$ backscattering phonons, the sum of similar expressions should be used.

As for the second term in Eq. (1), when the conductivity is determined by fluctuations in the voltage across the tunneling junctions between SWCNT bundles, it can be written [40] in the form

$$\rho_2(T) = \rho_t \exp\left(\frac{T_t}{T + T_s}\right).$$

Here again, ρ_t is independent of the temperature constant. The parameter T_t has the order of magnitude corresponding to typical barrier energies $E_t \sim k_B T_t$. It determines the behavior of the system at high temperatures, when the thermal voltage fluctuation become large enough. The ratio T_t/T_s determines the tunneling in the absence of fluctuations (the low-temperature limit).

The mathematical treatment of the experimental data involved the approximation of normalized dependencies $R(T)/R(300\text{ K})$ using the least-squares procedure by the sum of two functions:

$$R(T)/R(300\text{ K}) = F_1(T) + F_2(T). \qquad (2)$$

The first function

$$F_1(T) = \sum_i^N A_{mi} \exp\left(-\frac{T_{mi}}{T}\right) \qquad (3)$$

is related to SWCNT contribution into the full resistance (N is the number of conducting channels in SWCNT bundles with peculiar frequencies of $2k_F$ backscattering phonons). The second function in Eq. (2),

$$F_2(T) = A_t \exp\left(\frac{T_t}{T + T_s}\right), \qquad (4)$$

is intended for FAT contribution.

In the course of approximation the values of parameters A_{mi}, T_{mi}, A_t, T_t, and T_s in Eqs. (3) and (4) were obtained. Note that all geometric factors in Eq. (1) are inside the temperature-independent constants A_{mi} and A_t. Besides, as

TABLE II. FAT parameters in Eq. (4) for pristine and doped SWCNT films with the transparency of about 90 and 70%.

	A_t	T_t	T_s	Adj.R^2	p_t
90%(prist.)	0.78	15.74	8.48	0.99977	0.82
90%(+I)	0.80	2.88	7.09	0.99977	0.81
90%(+CuCl)	0.75	2.03	8.83	0.99969	0.76
70%(prist.)	0.79	17.70	8.96	0.99933	0.84
70%(+I)	0.79	2.77	11.04	0.99899	0.80
70%(+CuCl)	0.75	2.60	12.14	0.99987	0.76

the normalized dependencies $R(T)/R(300\text{ K})$ are under treatment, the geometric factors of the sample itself are excluded. This made it possible to compare peculiar contributions into total resistance of SWCNT film.

The treatment itself was processed in two stages in order to diminish the number of adjustable parameters on every stage. At the first stage, the parameters A_t, T_t, and T_s in Eq. (4) were obtained for FAT tunneling between SWCNTs bundles. For this purpose the total normalized resistance was fitted to Eq. (4) at low temperatures in limited range: of 5 to 80 K for pristine films, and of 5 to 30–40 K for doped ones. This approach is justified by the fact that the SWCNT contribution in the total normalized resistance at low temperatures is exponentially small. The values of FAT parameters for pristine and doped SWCNT films with the transparency of 90 and 70% are given in Table II. In addition, the adjusted R^2 values in the least-squares procedure [43], and the relative values of FAT contribution p_t at temperature 300 K, when $R(T)/R(300\text{ K}) = 1$, are also given in this table.

At the second stage of the treatment, FAT contribution was extrapolated to the end temperature value $T = 300$ K using formula (4) with the values of parameters obtained at the fist stage, and then it was subtracted from the total normalized resistance $R(T)/R(300\text{ K})$. The remainder obtained was considered as normalized SWCNT contribution, which was in turn fitted to Eq. (3).

In the fitting process of SWCNT contribution according to the above-mentioned procedure it became clear that for pristine films this contribution can be well fitted to Eq. (3) with only one exponent ($N = 1$). It is illustrated in Fig. 4(a), where the total normalized resistance of pristine SWCNT film with the optical transparency ≈90% as well as its two constituents (FAT contribution and SWCNT part) are shown in the upper panel. As seen from the lower panel of Fig. 4(a), the SWCNT part is well enough approximated by Eq. (3) with one parameter $T_{m1} = 796$ K.

For doped films, it was revealed that no matter whether the iodine or the cuprous chloride was implied the SWCNT part could not be approximated by Eq. (3) with only one exponent. However, the good fit can be obtained when Eq. (3) is used with $N = 2$ for the iodine-doped films, and $N = 3$ for the cuprous chloride doped ones. It is illustrated by the data shown in Fig. 4(b) for the iodine-doped films, and in Fig. 4(c) for the CuCl-doped ones.

The summary parameters of SWCNT contributions for pristine and doped SWCNT films with the transparency of 90 and 70% are given in Table III.
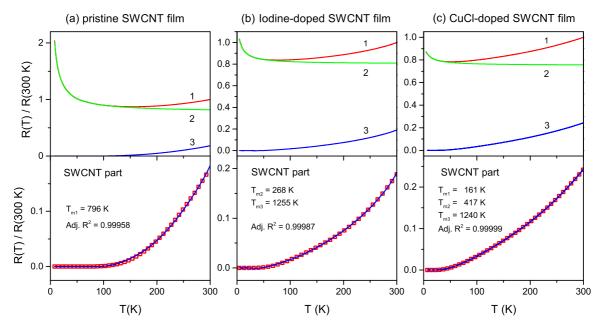
FIG. 4. The normalized resistance of (a) pristine, (b) iodine-doped, and (c) CuCl-doped SWCNT films. The upper panels show the total normalized resistance (1) and its two constituents: FAT contribution (2) and SWCNT part (3). The lower panels show the temperature dependency of the SWCNT part and its approximation by Eq. (3) (shown by square symbols). The optical transparency of the films is ≈90%.

As seen from the data given in Tables II and III, the values of parameters in Eqs. (3) and (4), as well as the relative values of SWCNT and FAT contributions, differ insignificantly for the films with optical transparency of about 90 and 70%. This means that the heterogeneous model we applied can be used in both cases of sparse and sufficiently dense SWCNT films. It is also seen that, at $T = 300$ K, the relative value of SWCNT contribution is only 24% in the most important case of the CuCl doping.

These data also clarify the impact of doping to the tunneling contribution to the electrical resistance of the films. Thus, the data presented in Table II demonstrate a significant decrease of T_t parameter value. As it was noted above, this value corresponds to the order of magnitude of the energy barriers for tunneling. After iodine doping of nanotubes it decreases 5.47 times; after CuCl doping it decreases even more—7.75 times (in both cases the film optical transparency is about 90%).

Thus, the separation of two contributions in frames of the heterogeneous model reveals the doping-induced magnitude reduction of both (nanotube and tunneling) contributions into the total film electrical resistance. The magnitude of the tunneling contribution decreases a bit more. Table IV shows

the data on the doping-induced reduction of the absolute values of the total electrical resistance of SWCNT film with transparency 90% and its nanotube and tunneling contributions (taken separately) at $T = 300$ K. It is seen, for instance, that while CuCl doping results in the total resistance reduction of 8.8 times (see Table. I), the magnitudes of tunneling and nanotube contributions reduce 9.5 times and 6.6 times, correspondingly.

IV. DISCUSSION

The observed picture of SWCNT constituents behavior as well as its variation upon doping can be interpreted in the framework of the above-mentioned model of phonon constraint of charge-carrier backscattering. For this purpose it is necessary to get the relationship between electronic and phonon structures of SWCNT.

Neglecting the curvature effects (which is a reasonable approximation for large-diameter nanotubes, investigated experimentally), the SWCNT electronic band structure can be obtained from the energy bands of a graphene sheet via application of periodic boundary conditions upon the wave vector (the so-called zone-folding approach). The π-orbital dispersion relation of graphene within the orthogonal

TABLE III. The nanotube part parameters in Eq. (3) for pristine and doped SWCNT films with the transparency of 90 and 70%.

	A_{m1}	T_{m1}	A_{m2}	T_{m2}	A_{m3}	T_{m3}	Adj.R^2	p_n
90%(prist.)	2.52	796					0.99958	0.18
90%(+I)			0.24	268	5.85	1255	0.99987	0.19
90%(+CuCl)	0.14	161	0.36	417	4.46	1240	0.99999	0.24
70%(prist.)	3.33	910					0.99933	0.16
70%(+I)			0.21	211	6.25	1252	0.99937	0.20
70%(+CuCl)	0.14	158	0.46	481	4.30	1248	0.99999	0.24

TABLE IV. The doping-induced decrease of the total electrical resistance and its tunneling and nanotube components for nanotube films at $T = 300$ K. The values are expressed in terms of the ratio to the corresponding values for pristine films. The film optical transparency is about 90%.

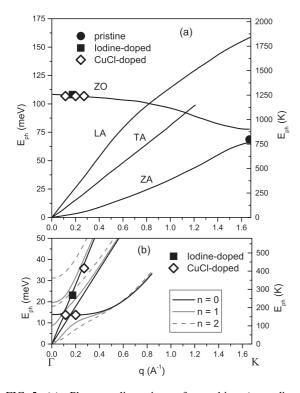|	Total resistance	Tunneling	Nanotubes
Iodine doped	5.72	5.78	5.41
CuCl doped	8.80	9.50	6.60

FIG. 5. (a) Phonon dispersion of graphite (according to Refs. [46–48]). (b) Low-energy phonon dispersion of 2-nm-diameter SWCNT, calculated from continuous theory [49]. The resulting $2k_F$ phonons concerned with backscattering of charge carriers in SWCNT are shown on both panels by corresponding symbols.

nearest-neighbor tight-binding method has the form

$$E^{\pm}(k_x, k_y) = \pm\gamma\sqrt{1 + 4\cos\frac{\sqrt{3}k_x a}{2}\cos\frac{k_y a}{2} + 4\cos^2\frac{k_y a}{2}},$$

$$(5)$$

where γ is a hopping parameter, describing the interaction between two neighboring carbon atoms and equal to 2.9 eV; k_x and k_y are Cartesian components of the electron wave vector; and a is a graphene lattice constant equal to 2.49 Å. The dispersion relation of a SWCNT corresponds to Eq. (5) with the difference that the electronic wave vector remains quasicontinuous only along the tube axis, but becomes discrete in the circumferential direction. The resulting electronic structure is described with a set of "cutting lines," each of which corresponds to an electron sub-band of the SWCNT [44,45]. If such lines cross the points $\mathbf{K} = (2\pi/\sqrt{3}a, 2\pi/3a)$ and $\mathbf{K}' = (2\pi/\sqrt{3}a, -2\pi/3a)$ of the graphene hexagonal Brillouin zone, the SWCNT is metallic, otherwise it is semiconducting.

Figures 6 and 8 show the electronic dispersions for metallic (14,14) and semiconducting (25,0) nanotubes, together with the densities of states for all the nanotubes with diameters in the range of 1.9–2.1 nm, obtained with use of Eq. (5) and the zone-folding approach.

The high-frequency phonon spectra of the SWCNT might be also described within the zone-folding scheme [the dispersion of some phonon bands of graphite is shown in Fig. 5(a)] [46–48]. At the same time, the low-energy phonon

branches in the SWCNT differ significantly from the ones of graphite. For a quantitative description of these phonons we use a continuous model [49], which has been applied for the study of low-temperature specific heat of the carbon nanotubes [50]. Within this model the phonon state is determined with a 3×3 dynamic matrix, the structure of which depends on the phonon wave vector q and a discrete wave number n. During the intra-sub-band scattering process only the continuous electron wave vector is changed, while the discrete wave number along the circumference remains the same. Thus, only $n = 0$ phonons participate in such processes. For these vibrations the dynamical matrix from Ref. [49] has the solution for the twisting phonons (the twistons),

$$\omega = \sqrt{\frac{\mu}{\eta}}|q|, \qquad (6)$$

and for the mixed radial breathing (RBM) and longitudinal acoustic (LA) modes

$$\omega_{1,2} = \frac{1}{\sqrt{2}}\sqrt{A_+ \pm \sqrt{A_-^2 + 4B^2}},$$

$$A_{\pm} = \left(\frac{\lambda}{\eta} + 2\frac{\mu}{\eta}\right)\left(\frac{1}{r^2} \pm q^2\right) + \frac{K}{\eta}\left(\frac{1}{r^2} - q^2\right)^2,$$

$$B = \frac{\lambda q}{\eta r}, \qquad (7)$$

where r is the SWCNT radius, λ and μ are two-dimensional analogs of the Lame coefficients, η is the surface mass density, and K is the bending rigidity. The parameter values are taken from Ref. [49]: $\lambda/\eta = 2400 \text{ cm}^{-2} \text{ nm}^2$, $\mu/\eta = 5200 \text{ cm}^{-2} \text{ nm}^2$, and $K/\eta = 12.5 \text{ cm}^{-2} \text{ nm}^4$. Within these units the SWCNT radius is given in nanometers and the resulting frequencies are given in cm^{-1}.

The band structure of the low-frequency phonons with $n = 0, 1, 2$ for the SWCNT with a diameter of 2 nm is given in Fig. 5(b). The results for $n = 1,2$ were obtained via numerical diagonalization of the dynamical matrix from Ref. [49].

The transport properties of the SWCNT are determined by electronic states near the Fermi level, which are located in the vicinity of the K and K' points of the graphene hexagonal Brillouin zone, where the energy bands have the form of touching Dirac cones. In the undoped SWCNT films the Fermi level lies close to the touching points of the linear dispersions and the main contribution to conductivity comes from metallic nanotubes due to the intervalley scattering between K and K' points via phonons near the K point of the phonon bands (Fig. 6) [51–54]. The approximation of $R(T)$ shows the contribution of phonons with energy of about 800 K (see Fig. 4). In the vicinity of the K point of the phonon band structure such energies correspond to the acoustic and optical bending modes (ZA and ZO) [see Fig. 5(a)]. We would like to mention that in Ref. [55] for samples of the pristine SWCNT network similar $R(T)$ measurements revealed the contribution of 1830 K phonons, which was attributed to the in-plane phonons also from the zone boundary.

In SWCNT films, doped with strong acceptors like iodine or CuCl, the Fermi level shifts inside the valence bands of semiconducting SWCNT, which start to contribute to the conductivity. In this situation, intra-sub-band processes due
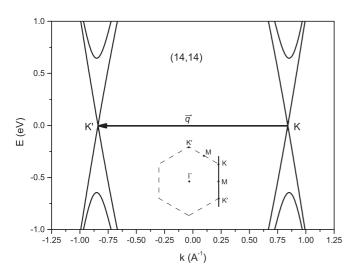
FIG. 6. Dispersions curves $E(k)$ for the M nanotube (14,14) near the points K and K' of the Brillouin zone. Inset: Brillouin zone of graphene in the basal plane where allowed k vectors along the K-K' direction are shown for the metallic sub-band of this nanotube by the bold line.

to the small wave-vector phonons start to play a role and each of the sub-bands, crossed by the Fermi level, may take part in the scattering. The $R(T)$ approximation shows the contribution of high-frequency phonons with energies about ≈ 1240 K and a set of low-frequency phonons. The phonons with high energy and small wave vectors correspond to the bending optical (ZO) phonons of graphene, which have weak q dependence.

To identify the origin of the low-energy phonons and to estimate the position of the Fermi level in doped SWCNTs, we first use an approximate electronic dispersion for the nanotube valence sub-band i of the form $E(k) = -v_F \sqrt{k^2 + (\frac{E_{ii}}{2v_F})^2}$, with v_F being the Fermi velocity equal to 6.264 eVÅ, and E_{ii} being the energy of the optical transition, seen in the absorption spectrum of pristine nanotube films. We thus do not specify the nanotube chirality at this point but rather take the band-structure parameters directly from the experiment (see optical absorption in Fig. 2). For the phonon wave vector, acting in the ith sub-band, we thus get the dependence on the Fermi energy position $q_i = 2k_F = \frac{2}{v_F}\sqrt{E_F^2 - (\frac{E_{ii}}{2})^2}$. Substituting this q into Eq. (7) we get the dependence of the phonon frequency on the Fermi energy. It should be mentioned that for the first metallic sub-band only twisting phonons may participate in the scattering [53,56].

The upper panel of Fig. 7 shows the density of states sketch for the first two metallic sub-bands (the massless sub-band and the sub-band, which leads to the optical transition with energy 1.32 eV) and the first two semiconducting sub-bands (the optical transition energies are 0.49 and 0.89 eV). The lower panel shows the dependence of the phonon energies of the 2-nm-diameter nanotube, which can contribute to the scattering within these sub-bands, on the position of the Fermi energy. The lowering of the Fermi level leads to the crossing of new sub-bands, which results in new phonons, available for scattering. The dashed horizontal lines in Fig. 7 depict the phonon energies, obtained from $R(T)$ fitting. The expected
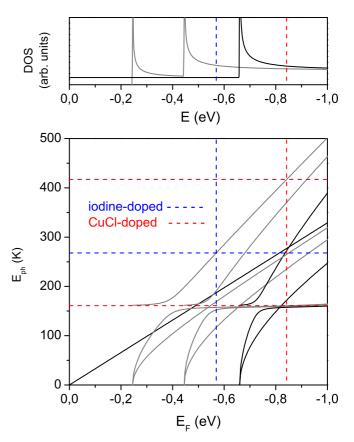

FIG. 7. Upper panel: the DOS sketch for the first two semiconducting (gray lines) and first two metallic (black lines) SWCNT valence sub-bands. The position of the Van Hove singularities corresponds to half of the electronic transition energies, visible in optical absorption. Lower panel: the dependence of the SWCNT phonon energies E_{ph}, which may participate in electron scattering on the position of the Fermi energy (E_F). Gray lines correspond to semiconducting sub-bands and black lines correspond to the metallic ones. The horizontal dashed lines depict the phonon energies, found from $R(T)$ approximation, and vertical dashed lines depict the corresponding Fermi levels.

position of the Fermi level is found from the crossing between these lines and the calculated phonon energies and from the optical absorption data. In the case of iodine-doped SWCNTs, the optical spectra show the suppression of the E_{11S} and, partially, E_{22S} transitions. The corresponding Fermi energy is located at $E_F \approx -0.6$ eV. In the case of CuCl-doped SWCNTs we have two low-energy contributions, and the optical spectra show the suppression of both semiconducting and first metallic transitions, which corresponds to the Fermi level of $E_F \approx -0.85$ eV.

Until now we did not include the nanotube chirality in our study and relied solely on model dispersion based on the nanotube electronic band shape and optical transition energies, observed in experiment. To investigate the influence of chirality on the Fermi level position we calculate the band structures with the tight-binding dispersion (5) and periodic boundary conditions [44,45] for all possible SWCNT geometries with diameters in the range of 1.9–2.1 nm. We then determine the Fermi energies via a FORTRAN code by
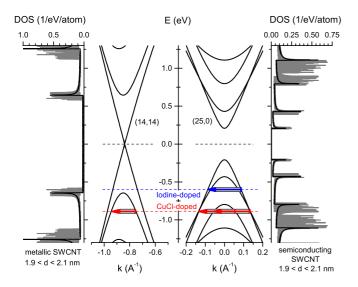
FIG. 8. Outside: DOS for all metallic (left) and semiconducting (right) SWCNT with diameters over 1.9–2.1-nm range. Inside: The dispersion curves $E(k)$ for metallic (14,14) and semiconducting (25,0) SWCNT (as an example). The Fermi levels at $0, -0.6$, and -0.9 eV for pristine, iodine-doped, and CuCl-doped SWCNT films correspondingly are denoted with the dotted lines. The resulting values of $2k_F$ phonons concerned with backscattering of charge carriers in SWCNT are shown by arrows.

matching the electronic bands with the phonon wave vectors, corresponding to the phonon energies, found during $R(T)$ approximation. The results for the most symmetric metallic (14,14) and semiconducting (25,0) nanotubes are shown in Fig. 8 together with the DOS of all the tubes used for the calculations of Fermi energy positions. The widths of the arrows in Fig. 8, which connect two points of the electronic dispersions and represent the phonon wave vectors, correspond to the spread of the obtained Fermi levels for different tube chiralities. The phonon modes, which match the energies from Table III (T_{m1} and T_{m2}) and the wave-vector lengths from Fig. 8, are marked in Fig. 5(b) and are attributed to the low-energy LA and RBM modes of the SWCNT. The obtained E_F is ≈ -0.6 eV for iodine-doped nanotubes and ≈ -0.9 eV for CuCl-doped ones. The small difference in the case of the CuCl-doping result as compared to the analytically obtained ≈ -0.85 eV arises from the use of the more accurate tight-binding dispersion. It is worth mentioning that, if the inter-sub-band scattering by phonons with $n \neq 0$ is taken into account, the resulting E_F positions may change by ≈ 0.1 eV.

At the same time, since the studied samples contain nanotubes which, most probably, have different filling ratios, and the relative position of the Fermi level may differ for each nanotube, a more detailed study of the low-energy phonon contributing to resistivity is not reasonable. The main result, however, is the observation of low-energy phonon contribution in the $R(T)$ behavior of the nanotube films, which arises as a result of SWCNT doping due to the shift of the Fermi level inside the valence band.

V. CONCLUSION

The transparent conducting netlike films of single-wall carbon nanotubes of large average diameter (≈ 2 nm) have been prepared for making transparent conducting electrodes for photovoltaic devices or displays. Their electrical conducting properties appeared to be very interesting from the fundamental point of view. As a result it has been shown that the electrical resistance drop, caused by doping of SWCNTs via filling the tube internal channel with iodine or CuCl, occurs because the Fermi level is shifted into the valence band to significant value: ≈ -0.9 eV in the case of doping with CuCl. Such CuCl-doped SWCNT films have $R_{sq} \approx 100$ ohm at room temperature. This value is already comparable with R_{sq} values for indium tin oxide being today the most used practical material. It should be noted, however, that the nanotube contribution in total resistance of such films is only 24% (see Table III). At low temperatures, conducting properties of the nanotube contribution are determined by participation of low-energy (150–400 K) phonons in the backscattering process. However, it exerts no noticeable influence on the relative value of nanotube contribution at room temperature.

In addition, the data obtained give evidence that the doping decreases not only the magnitude of nanotube contribution but also (and in a greater degree) the magnitude of tunneling contribution to the total resistance of SWCNT films. It happens due to a strong doping-induced decrease of the energy barriers for charge-carrier tunneling between the bundles of nanotubes.

[1] Z. Wu, Z. Chen, X. Du, J. M. Logan, J. Sippel, M. Nikolou, K. Kamaras, J. R. Reynolds, D. B. Tanner, A. F. Hebard, and A. G. Rinzler, Science **305**, 1273 (2004).

[2] L. Hu, D. S. Hecht, and G. Grüner, Nano Lett. **4**, 2513 (2004).

[3] A. D. Pasquier, H. E. Unalan, A. Kanwal, S. Miller, and M. Chhowalla, Appl. Phys. Lett. **87**, 203511 (2005).

[4] G. Gruner, J. Mater. Chem. **16**, 3533 (2006).

[5] M. W. Rowell, M. A. Topinka, M. D. McGehee, H.-J. Prall, G. Dennler, N. S. Sariciftci, L. Hu, and G. Gruner, Appl. Phys. Lett. **88**, 233506 (2006).

[6] J. van de Lagemaat, T. M. Barnes, G. Rumbles, S. E. Shaheen, T. J. Coutts, C. Weeks, I. Levitsky, J. Peltola, and P. Glatkowski, Appl. Phys. Lett. **88**, 233503 (2006).

[7] D. Zhang, K. Ryu, X. Liu, E. Polikarpov, J. Ly, M. E. Tompson, and C. Zhou, Nano Lett. **6**, 1880 (2006).

[8] H. E. Unalan, G. Fanchini, A. Kanwal, A. Du Pasquier, and M. Chhowalla, Nano Lett. **6**, 677 (2006).

[9] A. Kaskela, A. G. Nasibulin, M. Y. Timmermans, B. Aitchison, A. Papadimitratos, Y. Tian, Z. Zhu, H. Jiang, D. P. Brown, A. Zakhidov, and E. I. Kauppinen, Nano Lett. **10**, 4349 (2010).

[10] N. Hamada, S.-i. Sawada, and A. Oshiyama, Phys. Rev. Lett. **68**, 1579 (1992).

[11] R. Saito, M. Fujita, G. Dresselhaus, and M. S. Dresselhaus, Phys. Rev. B **46**, 1804 (1992).

[12] R. Saito, M. Fujita, G. Dresselhaus, and M. S. Dresselhaus, Appl. Phys. Lett. **60**, 2204 (1992).

[13] P. E. Lyons, S. De, F. Blighe, V. Nicolosi, L. F. C. Pereira, M. S. Ferreira, and J. N. Coleman, J. Appl. Phys. **104**, 044302 (2008).

[14] J. H. Yim, Y. S. Kim, K. H. Koh, and S. Lee, J. Vac. Sci. Technol. **26**, 851 (2008).

[15] K. Mustonen, P. Laiho, A. Kaskela, T. Susi, A. G. Nasibulin, and E. I. Kauppinen, Appl. Phys. Lett. **107**, 143113 (2015).

[16] A. Kaskela, P. Laiho, N. Fukaya, K. Mustonen, T. Susi, H. Jiang, N. Houbenov, Y. Ohno, and E. I. Kauppinen, Carbon **103**, 228 (2016).

[17] V. L. Kuznetsov, A. N. Usoltseva, A. L. Chuvilin, E. D. Obraztsova, and J.-M. Bonard, Phys. Rev. B **64**, 235401 (2001).

[18] D. S. Hecht, A. M. Heintz, R. Lee, L. Hu, B. Moore, C. Cucksey, and S. Risser, Nanotechnology **22**, 075201 (2011).

[19] K. Mustonen, P. Laiho, A. Kaskela, Z. Zhu, O. Reynaud, N. Houbenov, Y. Tian, T. Susi, H. Jiang, A. G. Nasibulin, and E. I. Kauppinen, Appl. Phys. Lett. **107**, 013106 (2015).

[20] L. Grigorian, K. A. Williams, S. Fang, G. U. Sumanasekera, A. L. Loper, E. C. Dickey, S. J. Pennycook, and P. C. Eklund, Phys. Rev. Lett. **80**, 5560 (1998).

[21] B. B. Parekh, G. Fanchini, G. Eda, and M. Chhowalla, Appl. Phys. Lett. **90**, 121913 (2007).

[22] A. A. Tonkikh, V. I. Tsebro, E. A. Obraztsova, K. Suenaga, H. Kataura, A. G. Nasibulin, E. I. Kauppinen, and E. D. Obraztsova, Carbon **94**, 768 (2015).

[23] E. D. Obraztsova, A. A. Tonkikh, P. V. Fedotov, E. A. Obraztsova, V. I. Tsebro, A. A. Dolgoborodov, A. G. Nasibulin, E. I. Kauppinen, and A. L. Chuvilin, in The Fifteenth International Conference on the Science and Application of Nanotubes (NT-14), 2014 (unpublished).

[24] A. A. Tonkikh, V. I. Tsebro, A. A. Dolgoborodov, E. A. Obraztsova, A. G. Nasibulin, E. I. Kauppinen, H. Kataura, K. Suenaga, A. L. Chuvilin, and E. D. Obraztsova, in The Fourth International Workshop on Nanocarbon Photonics and Optoelectronics, 2014 (unpublished).

[25] R. Pfeiffer, H. Kuzmany, F. Simon, S. N. Bokova, and E. Obraztsova, Phys. Rev. B **71**, 155409 (2005).

[26] X. Fan, E. C. Dickey, P. C. Eklund, K. A. Williams, L. Grigorian, R. Buczko, S. T. Pantelides, and S. J. Pennycook, Phys. Rev. Lett. **84**, 4621 (2000).

[27] L. Guan, K. Suenaga, Z. Shi, Z. Gu, and S. Iijima, Nano Lett. **7**, 1532 (2007).

[28] A. A. Eliseev, L. V. Yashina, N. I. Verbitskiy, M. M. Brzhezinskaya, M. V. Kharlamova, M. V. Chernysheva, A. V. Lukashin, N. A. Kiselev, A. S. Kumskov, B. Freitag *et al.*, Carbon **50**, 4021 (2012).

[29] A. B. Kaiser, G. Düsberg, and S. Roth, Phys. Rev. B **57**, 1418 (1998).

[30] A. B. Kaiser, Rep. Prog. Phys. **64**, 1 (2001).

[31] A. Znidarsic, A. Kaskela, P. Laiho, M. Gaberscek, Y. Ohno, A. G. Nasibulin, E. I. Kauppinen, and A. Hassanien, J. Phys. Chem. C **117**, 13324 (2013).

[32] A. Moisala, A. G. Nasibulin, D. P. Brown, H. Jiang, L. Khriachtchev, and E. I. Kauppinen, Chem. Eng. Sci. **61**, 4393 (2006).

[33] A. A. Tonkikh, E. D. Obraztsova, E. A. Obraztsova, A. V. Belkin, and A. S. Pozharov, Phys. Status Solidi B **249**, 2454 (2012).

[34] P. V. Fedotov, A. A. Tonkikh, E. A. Obraztsova, A. G. Nasibulin, E. I. Kauppinen, A. L. Chuvilin, and E. D. Obraztsova, Phys. Status Solidi B **251**, 2466 (2014).

[35] E. Burstein, Phys. Rev. **93**, 632 (1954).

[36] T. S. Moss, Proc. Phys. Soc. B **67**, 775 (1954).

[37] H. Kataura, Y. Kumazawa, Y. Maniwa, I. Umezu, S. Suzuki, Y. Ohtsuka, and Y. Achiba, Synth. Met. **103**, 2555 (1999).

[38] R. Saito, G. Dresselhaus, and M. S. Dresselhaus, Phys. Rev. B **61**, 2981 (2000).

[39] R. B. Weisman and S. M. Bachilo, Nano Lett. **3**, 1235 (2003).

[40] P. Sheng, Phys. Rev. B **21**, 2180 (1980).

[41] S. Kivelson and A. J. Heeger, Synth. Met. **22**, 371 (1988).

[42] A. B. Kaiser, Phys. Rev. B **40**, 2806 (1989).

[43] D. A. Ratkowsky, *Handbook of Nonlinear Regression Models* (Marcel Dekker, New York, 1990).

[44] R. Saito, G. Dresselhaus, and M. S. Dresselhaus, *Physical Properties of Carbon Nanotubes* (Imperial College, London, 1999).

[45] G. G. Samsonidze, R. Saito, A. Jorio, M. A. Pimenta, A. G. Souza Filho, A. Grüneis, G. Dresselhaus, and M. S. Dresselhausa, J. Nanosci. Nanotechnol. **3**, 431 (2003).

[46] S. Siebentritt, R. Pues, K.-H. Rieder, and A. M. Shikin, Phys. Rev. B **55**, 7927 (1997).

[47] V. N. Popov and P. Lambin, Phys. Rev. B **73**, 085407 (2006).

[48] M. Mohr, J. Maultzsch, E. Dobardžić, S. Reich, I. Milošević, M. Damnjanović, A. Bosak, M. Krisch, and C. Thomsen, Phys. Rev. B **76**, 035439 (2007).

[49] S. B. Rochal, V. L. Lorman, and Y. I. Yuzyuk, Phys. Rev. B **88**, 235435 (2013).

[50] M. V. Avramenko and S. B. Roshal, Phys. Solid State **58**, 1011 (2016).

[51] P. L. McEuen, M. Bockrath, D. H. Cobden, Y.-G. Yoon, and S. G. Louie, Phys. Rev. Lett. **83**, 5098 (1999).

[52] T. Ando and T. Nakanishi, J. Phys. Soc. Jpn. **67**, 1704 (1998).

[53] T. Ando, T. Nakanishi, and R. Saito, J. Phys. Soc. Jpn. **67**, 2857 (1998).

[54] S. Reich, C. Thomsen, and J. Maultzsch, *Carbon Nanotubes, Basic Concepts and Physical Properties* (Wiley-VCH, Berlin, 2004).

[55] V. Skákalová, A. B. Kaiser, Y.-S. Woo, and S. Roth, Phys. Rev. B **74**, 085403 (2006).

[56] C. L. Kane, E. J. Mele, R. S. Lee, J. E. Fischer, P. Petit, H. Dai, A. Thess, R. E. Smalley, A. R. M. Verschueren, S. J. Tans, and C. Dekker, Europhys. Lett. **41**, 683 (1998).